Indian J. Phys. **75A** (6), 607-614 (2001)

IJP A
— an international journal

Correlation between microstructure and mechanical property of industrial Cu-Mn-Zn alloys : effect of transitional solute Mn

H Dutta[1], S K Pradhan*[1] and M De[2]

[1]Department of Physics, The University of Burdwan, Golapbag, Burdwan-713 104, West Bengal, India

[2] Department of Materials Science, Indian Association for the Cultivation of Science, Jadavpur, Calcutta-700 032, India

E-mail skpbu@dte vsnl net in

Received 17 May 2001, accepted September, 2001

Abstract Eight compositions of Cu-Mn-Zn alloy in α-phase and mixed-phase (α + β) regions have been analysed both in the annealed and cold-worked states employing Rietveld's powder structure refinement method and Warren-Averbach's method of X-ray line profile analysis. The detailed microstructure has been analyzed in terms of several parameters depicting lattice imperfections like, stacking faults, particle sizes (coherently diffracting domain), r.m.s. strains, dislocation densities, lattice parameter change *etc*. A specially prepared Si standard has been used in the Rietveld software for accurate estimation of instrumental broadening in the peak-broadening analysis. Grain size and shape, grain-boundary structures and several other metallographic features are obtained from optical microscopy studies. Vickers' microhardness values are measured and finally, different correlations amongst various parameters obtained from these studies are established. It is interesting to observe that the defect microstructures of the Cu-Zn-Mn alloys are primarily controlled by the presence of transitional solute Mn which precipitates continuously and discontinuously inside the grain, at the grain-boundary or in the form of dendritic networks.

Keywords Cu-Mn-Zn alloy, Rietveld analysis, structure-property analysis

PACS Nos. 61.72.-y, 62.20.Fe, 81.40.Lm

1. Introduction

Materials with desired properties can be obtained by controlling the defect microstructure and the microstructure of a material can be well characterized from an analysis of X-ray powder diffraction line profiles [1-8] that provides a nondestructive indirect method for obtaining a large number of microstructural parameters, like coherently diffracting domain (particle size), r.m.s. strain, stacking fault density, stacking fault energy, dislocation density, residual stress *etc*.

In the present study, eight compositions of a strongly non-corrosive ternary Cu-Mn-Zn alloys (industrially known as Cowles high manganese brass) have been chosen to monitor the influence of the transitional solute (Mn) on the defect sub-structure of binary Cu-Zn alloy. The defect microstructure of the alloys primarily has been characterized by employing Rietveld's powder structure refinement method [1-3] and Warren-Averbach's X-ray line profile analysis [5]. In an earlier study [9] on this alloy system, adopting only the Warren-Averbach's method [5], it was reported that the presence of the transitional solute Mn does not influence the microstructure of the alloys. But, its presence was said to impose some restrictions on further nucleation of defects in the lattice. In our recent work [10], the cold-worked state of the alloys was analyzed by employing X-ray profile fitting (individual profile) and modified Warren-Averbach's analysis [11]. The observations were however, quite different. Due to limitations of the said method of analysis, the microstructure of the annealed materials could not be properly characterised. To accomplish the microstructure of alloys both in annealed and cold-worked states as well as to estimate quantitatively the phase abundance in the multiphase alloys, we have adopted Rietveld's whole profile fitting power structure refinement method [1-3]. We have noticed by applying this improved technique of X-ray profile refinement that Mn plays a significant role in influencing the deformation microstructure of Cu-Mn-Zn alloys and the observation is further supplemented from the measure of mechanical property of hardness of the materials.

* Corresponding Author

2. Experimental

Following eight different compositions of ternary Cu-Mn-Zn alloy system in the Cu-solid solution (α-phase) range and in the mixed phase region $(\alpha+\beta(\alpha-Mn))$ were prepared from spectroscopically pure metals supplied by M/s Johnson, Matthey and Co., Ltd., London, following the same procedure as adopted earlier [9, 10]:

Cu- (1, 10, 20, 30) wt% Mn- 10 wt% Zn

and Cu- (1, 10, 20, 30) wt% Mn-20 wt% Zn.

After melting under vacuum in the temperature range of 1273-1423K, the alloy ingots were homogenized at about 2/3 of the melting temperature of the respective alloys, in the temperature range of 923-1023K for 10 days. No significant weight loss was detected except some grain recrystallization for prolonged heating. Cold-working by hand filing, obtaining annealed standard (723K for 10h) and preparation of flat diffractometer samples were made following the same procedures as adopted earlier [9, 10].

The X-ray powder diffraction profiles of both the cold-worked and annealed powder samples were recorded using Ni-filtered CuK_α radiation from a highly stabilized Philips X-ray generator (PW 1130) operating at 40 kV and 25 mA, coupled with a Philips X-ray powder diffractometer (PW 1710). The step-scan data (of step size 0.02^0 2θ and counting time 15-20s depending on the peak intensity) for entire angular range of the experimental samples were stored in a Philips PC, coupled with the powder diffractometer. A specially processed Si-powder sample [12] was used as instrumental standard in Rietveld's analysis [3].

3. Microstructure evolution by X-ray diffraction

Characterization of microstructure of the materials has been made employing both the Rietveld's whole profile fitting method [1-3] and modified Warren-Averbach's method [5,11]. For fitting of the experimental profiles, in the present study, the most suitable pseudo-Voigt analytical function [13] is adopted. An X-ray powder diffraction profile can be well described by a convolution relation [13]:

$$I_c(2\theta) = [B * (S * A)](2\theta) + bkg\,, \tag{1}$$

where * is the convolution symbol, 'bkg' is the fourth order polynomial function for background reproduction, $B(2\theta)$ is the true broadening of the profile, $S(2\theta)$ is the symmetric part of the instrumental profile and $A(2\theta)$ is asymmetric component of the instrumental profile;

$$A(2\theta) = \exp\left[-a_s\,|2\theta - 2\theta_0|\tan(2\theta_0)\right], \tag{2}$$

where a_s is the asymmetry parameter.

For both the $K\alpha_1$ and $K\alpha_2$ profiles, the $B(2\theta)$ and $S(2\theta)$ may be represented by the pseudo-Voigt function [13]:

$$pV(x) = \sum_{\alpha 1\alpha 2} I_{nl}\left[\eta C(x) + (1-\eta)\,G(x)\right], \tag{3}$$

where the Cauchyian component $C(x) = (1+x^2)^{-1}$ and the Gaussian component $G(x) = \exp\left[-(\ln 2)x^2\right]$ with $x = (2\theta - 2\theta_0)$ /HWHM and HWHM = ½ FWHM = $(U\tan^2\theta + V\tan\theta + W)^{1/2}$, where U, V and W are coefficients of the quadratic polynomial, η is the Gaussianity of X-ray peaks, θ_0 is the Bragg angle of $K\alpha_1$ peak and I_{nl} is the scale factor of the pV function [13].

The powder diffraction patterns were simulated providing all necessary structural information and some starting values of microstructural parameters of individual phases with the help of the software LS1 [3]. Initially, the positions of the peaks were corrected by successive refinements for systematic errors by taking into account the zero-shift error and sample displacement error (h), where $\Delta\theta_h = 2h\cos\theta / R$, R is the radius of the goniometer.

Considering the integrated intensity of the peaks, a function of structural parameters only, the Marquardt least squares procedures were adopted to minimize the difference between observed and simulated powder diffraction patterns [3]. The minimization is carried out by using the reliability index R_w (weighted residual error). The goodness of fit (GoF) is established by comparing R_W with R_{exp} leading to the value of $GoF = (R_w/R_{exp})^{1/2}$ [3,13].

The materials studied in the present case are multiphase. The Rietveld's method is now being successfully applied for determination of quantitative phase abundance of composite materials [13-16]. There is a simple relationship between the individual scale factors, determined considering all refined structural parameters of individual phases of a multiphase sample, and the phase concentration (volume fraction) in the mixture. The weight fraction (W_i) for each phase obtained from the refinement relation is:

$$W_i = S_i(ZMV)_i \,/\, \sum S_i(ZMV)_i \tag{4}$$

where S_i, M_i, Z and V_i are the scale factor, the number of molecules per unit cell, the molecular weight and unit-cell volume of phase i, and the summation is over all phases present [3]. The structure refinement along with size-strain broadening was carried out simultaneously by adopting the standard procedure [3]. An improvised approach [14] has also been considered in the present study to estimate the anisotropy in crystallite size and microstrain from the size-strain separation analysis.

3.1 Size-strain analysis :

The basic consideration of this method is the modeling of the diffraction profiles (broadened due to instrumental settings, small particle size and r.m.s. microstrain) by an analytical function (pseudo-Voigt) which is a combination of Cauchyian, Gaussian and asymmetry functions as well [13]. Being a linear combination of Cauchyian and Gaussian functions, the pV function is the most reliable peak-shape function and is being widely used in Rietveld structure refinement software [3, 6-11, 13]. Following the single-peak method for Fourier analysis [11], the particle size (D) and r.m.s. strain ($< \varepsilon^2 >^{1/2}$) values in different directions have been obtained. Due to anisotropy in particle size and microstrain values, profiles with different Miller indices are broadened in different manner and this effect frequently creates problems in Rietveld structure refinement [3]. To consider the influence of anisotropy in particle size and r.m.s. strain values in the profile shapes, the tensors similar to the temperature factors, for particle sizes and microstrains in different crystallographic directions, have been used [3].

By using the LS1 software [3] and following the methodology as outlined above, the Rietveld analysis [1-3] has been made to study the microstructure of single and multiphase materials. Profile refinement continues until convergence is reached in each case, with the value of the quality factor (GoF) approaching 1. The typical output of the above analysis contains information regarding anisotropic/effective $(D_e)_{hkl}$ and $(< \varepsilon^2 >^{1/2})_{hkl}$, lattice parameter, atomic positions, occupancy factors, temperature factors, preferred orientations *etc*. Taking the results of this analysis, the defect microstructure of the materials in terms of other types of lattice imperfections, has been obtained in the following way :

(i) The compound fault probability parameters for Cu-Mn-Zn (fcc) phases have been estimated by adopting the Warren-Averbach broadening analysis [5] and employing the following relevant expression .

$$.5(\alpha' + \alpha'') + \beta = 1.76a[D_{111} - D_{100}]/D_{111}D \qquad (5)$$

where a is the lattice parameter, α' and α'' are intrinsic and extrinsic stacking faults probabilities respectively, β is twin faults probabilities, [5, 9, 10] and D's are the particle sizes in different directions.

(ii) Using the values of particle sizes and r.m.s strains, the dislocation density (ρ) values have been evaluated [15] following the same procedure as adopted earlier in some recent X-ray line broadening analyses [7-10] :

$$\rho = (\rho_D \, \rho_S)^{1/2} \qquad (6)$$

where ρ_D (due to particle size) = $3/D^2$ and ρ_S (due to strain broadening) = $K < \varepsilon_L^2 > /b^2$, where $< \varepsilon_L^2 >$ is the mean squared microstrain, $K = 6\pi$ for Gaussian strain distribution and b is the Burgers vector and its value is $a/\sqrt{2}$ for [110] direction of the fcc structure.

4. Results and discussion

Figure 1 (a) shows some X-ray powder diffraction patterns of annealed and cold-worked Cu-Mn-Zn alloys. It is evident from the figure that cold-worked profiles are broadened than their annealed counterpart. Figure 1(b) shows a typical Rietveld's refined X-ray power diffraction pattern of annealed Cu-30Mn 20Zn alloy. The pattern reveals that the alloys are prepared in mixed phase region – primary phase is Cu base Cu Zn-Mn alloy

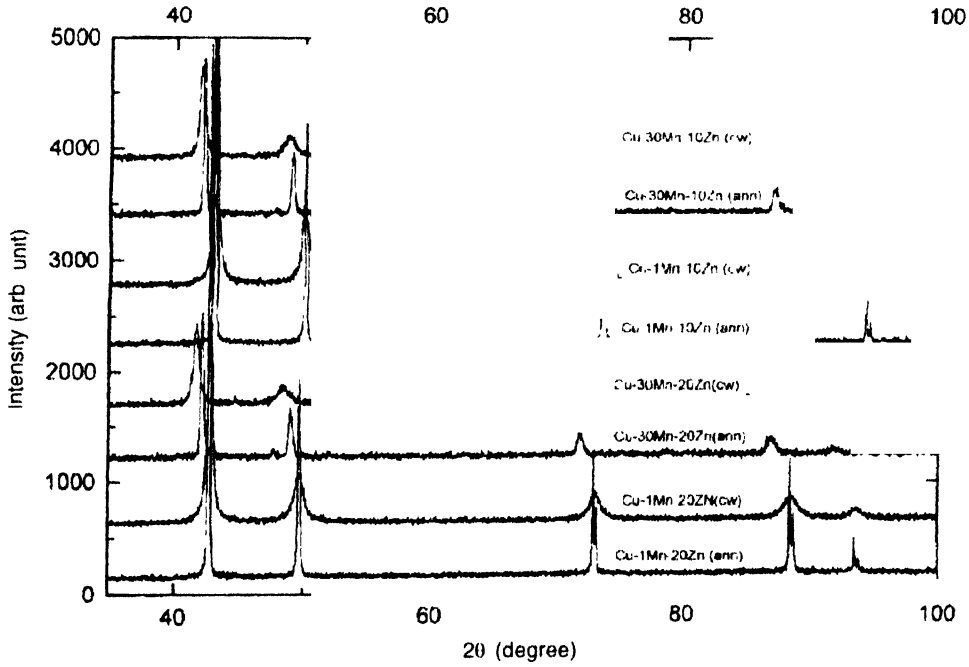

Figure 1(a). X-ray powder diffraction patterns of some annealed and cold-worked Cu Mn-Zn alloys

(fcc) and the secondary phase is α-Mn (A12; cubic). As α-Mn lines are very close to the lines of primary phase (inset), the Warren-Averbach's Fourier method [5] fails to analyze these

(α') and extrinsic (α'') nature, (b) change in lattice parameter ($\Delta a / a_0$) and (c) long range residual stress (σ). As both the effects of the residual stress and lattice parameter change are

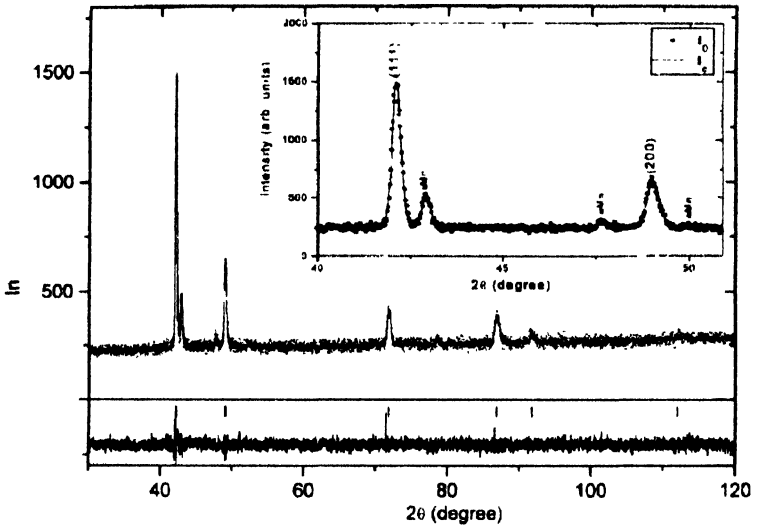

Figure 1(b). X-ray powder diffraction pattern of annealed Cu 30Mn-20Zn (I_0) refined by Rietveld's whole profile fitting analysis (I_c)

Inset magnified critical region showing nearly overlapping peaks of two phases

overlapping peaks. The Rietveld's whole profile refinement method [1-3] adopted in the present study, not only ensures very accurate estimation of backgrounds of overlapping reflections but also provides estimations of individual phases and thereby giving very accurate results of the microstructural parameters of each phase. The GoF values of Rietveld's analysis of total sixteen samples vary from 1.0 to 1.14, indicating high accuracy in the structure refinement analysis.

4.1 Peak shift analysis :

The relative peak-shifts between successive pairs of reflections of annealed standard and cold-worked samples having fcc structure, give information regarding (a) stacking faults of intrinsic

very small for powdered materials [6-10], the peak-shift analysis has been done by (i) considering the entire peak shift solely due to deformation stacking fault probability $<\alpha>=(\alpha'-\alpha'')$ alone, (ii) considering the composite effects of lattice parameter change ($\Delta a / a_0$) and stacking fault probability $<\alpha>$ and the results are shown in Table 1. In the solid solution range, the peak-shift is mainly influenced by the concentration of stacking faults because ($\Delta a / a_0$) values are very small in comparison to $<\alpha>$ values. It is also evident that $<\alpha>$ values for Cu-Mn 10Zn alloys increase slowly with increasing Mn concentrations. The nature of variation is almost similar to binary Cu-Zn alloys [10, 15]. This observation is quite different from the earlier one [9], where the $<\alpha>$ values remain constant with increasing

Table 1. Microstructural parameters for cold-worked Cu-Mn-Zn alloys

Samples (wt%)	Lattice parameter (Å)		$\Delta a / a_0$	$\alpha = <\alpha'-\alpha''>$	$\alpha = <\alpha'-\alpha''>$ ($\Delta a / a_0 = 0$)	$1.5(\alpha'+\alpha'')+\beta$	
			× 10^3	× 10^3	× 10^3	× 10^3	
	a_{ann} (a_0)	a_{cw}				ann	cw
Cu-1Mn-10Zn	3.6403	3 6399	-0.05	6.23	4 89	0.72	40.67
Cu-10Mn-10Zn	3 6762	3.6778	-0.58	6.90	5.79	1 50	55.21
Cu-20Mn-10Zn	3.7116	3 7118	-0.14	8 95	9.82	0.00	58.20
Cu-30Mn-10Zn	3.7186	3 7325	3.27	9.01	12.46	0.22	68.80
Cu-1Mn-20Zn	3.6614	3.6662	0 85	7.93	8 23	0.93	68.86
Cu-10Mn-20Zn	3.6955	3.7015	1.17	8.09	8.69	1.76	74.82
Cu-20Mn-20Zn	3.7202	3.7325	2.07	8.91	9.86	1.68	77.39
Cu-30Mn-20Zn	3.7190	3.7533	8.01	9.07	15.27	2.08	79.13

Mn concentrations. For alloys with higher Mn concentration ($fcc+\alpha-Mn$), $<\alpha>$ values are quite high when contribution of ($\Delta a / a_0$) is neglected. However, considering the composite effect, $<\alpha>$ values follow up the above trend of variation but ($\Delta a / a_0$) values vary significantly, which implies that the peak shift in the mixed phase region is controlled by both these two effects. The change in ($\Delta a / a_0$) values has also been reflected in the change of lattice parameter values of annealed and cold-worked alloys (Table 1). For Cu-Mn-20Zn alloys, $<\alpha>$ values remain almost constant with increasing Mn concentrations and the nature of variation is quite similar to binary Cu-Mn alloy [16] as well as to the earlier studies [8-10]. Such variations in $<\alpha>$ values in higher Mn content Cu-30Mn-10Zn and Cu-30Mn-20Zn alloys may depict the influence of transitional solute in arresting the evolution of stacking faults [8-10]. The presence of α-Mn phase in the annealed samples is also evidenced in the respective X-ray diffraction patterns (Figures 1(a) and (b)); however, in the cold-worked patterns, α-Mn peaks could not be traced out due to overlapping results from peak broadening. The excess amount of Mn (α-Mn) along with their respective particle size and strain values in the mixed phase alloys have been estimated from the Rietveld's [3] analysis (Table 2).

Table 2. Microstructure of α-Mn in the mixed phase alloys

Sample (wt%)	Lattice parameter (A°)	Wt% (α Mn)	Particle size (A°)	Rms strain $\times 10^4$
Cu-30Mn-10Zn (ann)	8 5594	9 72	260	1 92
Cu-30Mn-10Zn (cw)	8 9367	2 07	80	26 42
Cu-30Mn-20Zn (ann)	8 6086	20 75	270	9 61
Cu-30Mn-20Zn (cw)	8 9479	5 86	34	46 16

4.2 Peak broadening analysis

For peak broadening analysis, a single line peak broadening technique is adopted in the Rietveld powder structure refinement method [3, 11]. In the present work, besides Rietveld's method, Warren-Averbach's method [5] of peak broadening

Table 3(a). Microstructural parameters of annealed powders of Cu-Mn-Zn alloys

Samples (wt%)	Particle size (Dc) (A°)		Strain $<\varepsilon_L^2>^{1/2}$ $\times 10^4$		D_{st} (A°)		Dislocation density (ρ) $\times 10^{10}$ (cm/cm^3)		ρ_{av} $\times 10^{10}$ (cm/cm^3)
	[111]	[100]	[111]	[100]	[111]	[100]	[111]	[100]	
Cu-1Mn-10Zn	790	726	0 0	0 0	11741	5084	0 004	0 004	0 004
Cu-10Mn-10Zn	670	580	0 0	0 0	5652	2447	0 006	0 005	0 006
Cu-20Mn-10zn	570	570	0 0	0 1	∞	∞	0 018	0 027	0 023
Cu-30Mn-10Zn	548	538	13 1	49 8	38684	16750	6 9	8 6	7 76
Cu-1Mn-20Zn	788	708	0 7	1 2	9131	3954	025	0 49	0 37
Cu-10Mn-20Zn	660	560	6 3	9 5	4841	2096	0 28	4.9	2 6
Cu-20Mn-20Zn	640	550	13 1	14 3	5120	2217	5 8	7 4	6 6
Cu-30Mn-20Zn	627	523	17 1	23 7	4129	1788	7 8	13 0	10 4

Table 3(b). Microstructural parameters of cold worked powders of Cu-Mn-Zn alloys

Samples (wt%)	Particle size (Dc) (A°)		Strain $<\varepsilon_L^2>^{1/2}>$ $\times 10^3$		D_{st} (A°)		Dislocation density (ρ) $\times 10^{11}$ (cm/cm^3)		ρ_{av} $\times 10^{11}$ (cm/cm^3)
	[111]	[100]	[111]	[100]	[111]	[100]	[111]	[100]	
Cu-1Mn-10Zn	175	83	2.1	3 5	207	89	3.5	12 2	7.9
Cu-10Mn-10Zn	156	67	2.9	4 9	154	67	5 3	21.2	13 3
Cu-20Mn-10zn	154	65	2 9	5.0	147	64	5 4	21 8	13 6
Cu-30Mn-10Zn	130	55	3 2	5 0	125	54	7 0	25.8	16 4
Cu-1Mn-20Zn	133	55	2 1	3 5	123	53	4 6	18 5	11 5
Cu-10Mn-20Zn	129	52	2.9	4.3	114	49	6 4	23 5	15 0
Cu-20Mn-20Zn	128	51	3.2	5.4	111	48	7 1	30.1	18.6
Cu-30Mn-20Zn	126	50	3.9	5.9	109	47	8.9	33 5	21 2

analyses is also considered for detailed analysis of defect microstructure of the alloys. From Rietveld analysis [1-3], anisotropic particle size (effective) $[D_e]_{hkl}$ and r.m.s. microstrains $[<\varepsilon_L^2>^{1/2}_{L=100\,A^0}]$ along [111] and [100] have been evaluated for all the alloy compositions both in annealed and cold-worked states. The evaluation of microstructure of annealed materials becomes possible adopting specially prepared Si [12] as instrumental standard. In this respect, Rietveld's method [3] gives much more information than any other classical method of peak broadening analysis. Moreover, it is also essential to know, to some extent, the microstructure of annealed materials for better estimation of the influence of cold-working on the defect microstructure. The results in detail for annealed and cold-worked materials, are tabulated in Tables (3(a) and 3(b) respectively.

From a comparative study of these tabulated results, it is evident that D_e values for cold-worked samples (Table 3(b)) decrease slowly with increasing Mn concentration and their values are smaller and much more anisotropic in nature than those from the annealed materials (Figure 2). The r.m.s. strain $<\varepsilon_L^2>^{1/2}$ values for cold-worked samples in general, are larger than those from the annealed materials and increase slowly with increasing solute concentration in the solid solution range. However, sudden increase in $<\varepsilon_L^2>^{1/2}$ values for annealed Cu-30Mn-10Zn and Cu-30Mn-20Zn (mixed phase) alloys, may be attributed to the generation of macrostress due to coherent growth of α-Mn phase because there may be a phase coherency or crystallographic orientation relationship between these two phases. Therefore, lots of line and planar defects such as dislocations and stacking faults, generated in the Cu-Mn-Zn solid solution may further act as nucleation sites of α-Mn. This type of coherent growth is quite common in mixed phase materials [17].

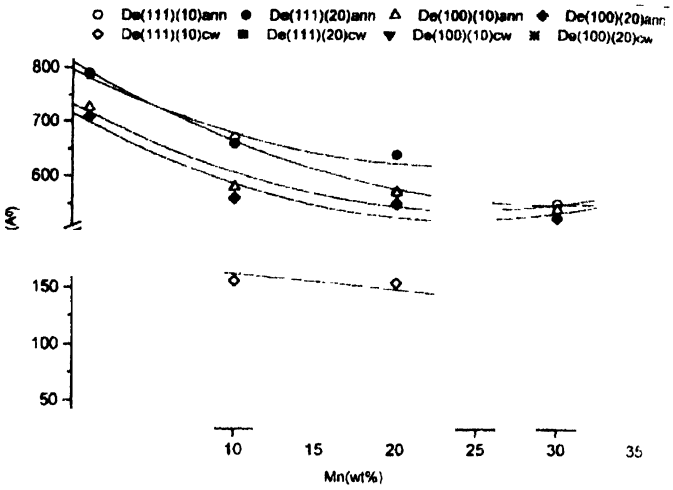

Figure 2. Plots of Mn composition vs particle size for annealed and cold worked Cu-Mn-Zn alloys

The stacking fault-dependent particle size (D_{sf}) values [8] decrease with increasing Mn and Zn concentrations (Tables 3(a) and 3(b)) and their values for annealed samples are quite high, which implies that the annealed materials are almost free

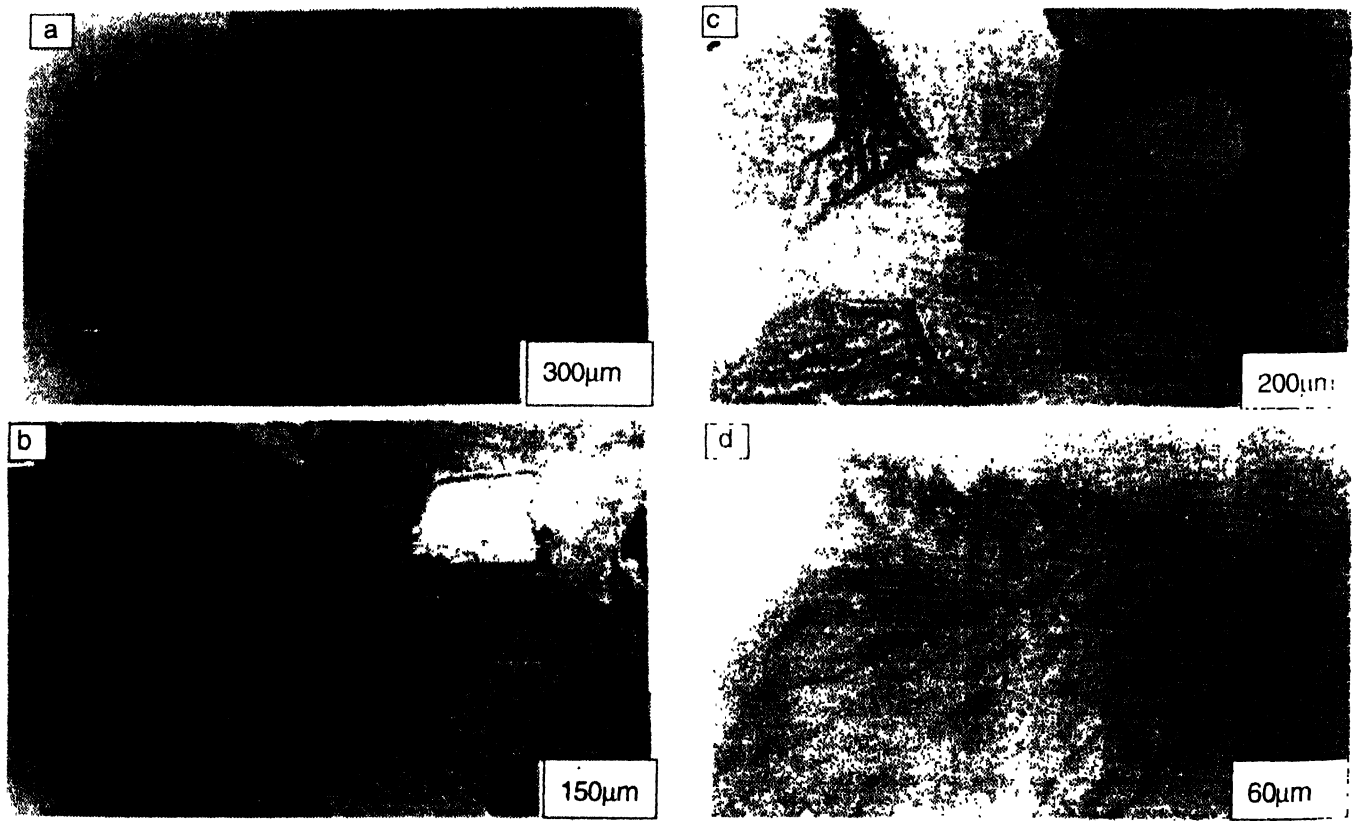

Figure 3. Optical micrographs of Cu-Mn-10Zn alloys : (a) sharp and clean grain boundaries (Cu-1Mn-10Zn), (b) inhomogeneous distribution of α-Mn precipitates (Cu-30Mn-10Zn). (c and d) particles α-Mn phase appeared as separate grains (Cu-30Mn-20Zn).

from stacking faults. The compound fault probability parameters $[1.5(\alpha'+\alpha'')+\beta]$ (Table 1) increase slowly with increasing solute concentrations and the cold-worked values are much more higher than their annealed counterpart, indicating significant influence of stacking faults towards size broadening. These variations are quite common for cold-worked fcc metallic alloys and corroborate the findings of the earlier observations [7-10]. The dislocation density (ρ) values of annealed and cold-worked materials are calculated using eq. (6) and shown in Tables 3(a) and 3(b). Like D_e and $< \varepsilon_L^2 >^{1/2}$ values, ρ values are also anisotropic in nature and for mixed phase annealed alloys, ρ values are quite high in comparison to the solid solution alloys, which further confirms the accumulation of dislocations in mixed phase materials. To the authors' knowledge, such type of observations of microstructure in annealed and cold-worked materials have not been reported earlier. Unlike the earlier observation [9], ρ values increase with increasing solute concentration, which depicts the influence of solute on the microstructure of the alloy system. The average dislocation density (ρ_{av}) values for annealed materials increases from 0.4 to 1039×10^8 cm/cm^3 and that for cold-worked materials increases from 7.874 to 21.158 $\times 10^{11}$ cm/cm^3 with increasing solute (Mn+Zn) concentrations.

4.3 Optical microscopy and microhardness studies.

The optical micrographs (Figure 3) were obtained using a (Carl Zeiss) high resolution optical microscope, following the procedure as adopted earlier [7-10]. For microhardness studies, same etched discs were used and the microhardness values were measured following the earlier procedure [7-10] using Vickers microhardness tester attached to the said optical microscope. The values of the microhardness (H_v) have been reported elsewhere [10] and considered here for establishing structure-property correlation of bulk annealed and cold-worked alloys.

It is observed that the α-phase grains, in general, were reduced in size with increasing solute concentrations and grain boundaries of single phase alloys were sharp and clean (Figure 3(a)). The microstructures of mixed phase alloys are somewhat different. In Cu-30Mn-10Zn, grain boundaries are quite sharp and the excess α-Mn particles are unevenly distributed as precipitates over the α-phase grains (Figure 3(b)). In Cu-30Mn-20Zn, the grain boundaries are quite wide due to growth of secondary phase α-Mn, primarily at the grain boundaries (Figures 3(c, d)). The presence of α-Mn peaks in X-ray diffraction patterns (Figures 1(a) and 1(b)) also corroborates the findings of optical microscopy.

Figure 4 shows the variations of average dislocation density, ρ_{av} and average particle size D_{av}, both for annealed and cold-worked α-phase alloy. The variation of microhandness H_v *vs* stacking fault probability, $< \alpha >$ against microhardness H_v was shown earlier [10]. These plots depict the nature of interrelation between the microstructure and mechanical property of the alloys measured from two different methods of analyses.

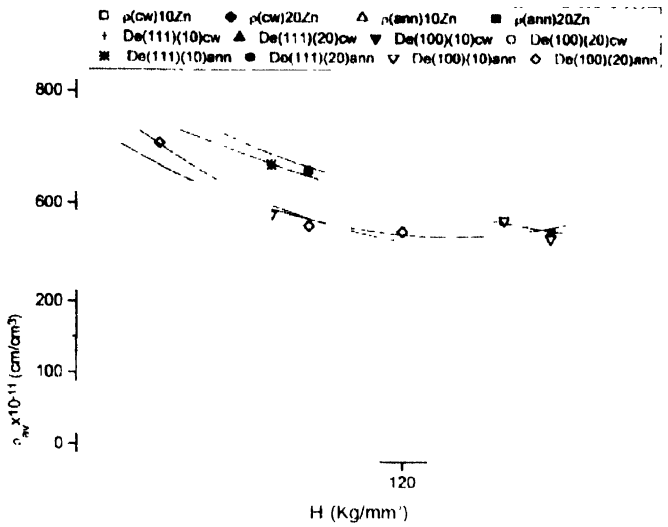

Figure 4. Plots of ρ_{av} and D_{av} *vs* Vickers' microhardness H_v for Cu-Mn-Zn alloys.

5. Conclusion

The above study on structure-property correlation of Cu-Mn-Zn alloys leads to the following important conclusions:

(i) The defect microstructure of mixed phase materials can be characterized in a better way using simultaneously the Rietveld's and Warren-Averbach's methods of analysis rather than any single method of X-ray analysis.

(ii) Both the solutes Mn and Zn control the microstructure of the ternary (α-phase) alloys with Mn exerting stronger influence.

(iii) In multiphase alloy compositions with increasing Mn and Zn concentrations, the microstructure is strongly influenced by the precipitation of α-Mn regions inside the α-phase grain and at the grain boundaries respectively.

(iv) Microhardness values H_v for multiphase alloy compositions are controlled by the formation of α-Mn phases.

(v) A close correlation could be established between the microstructure and mechanical property of the alloys from the results of XRD, optical microscopy and microhardness studies.

References

[1] H M Rietveld *Acta Cryst* **22** 151 (1967)

[2] H M Rietveld *J Appl Cryst* **2** 65 (1967)

[3] L Lutterotti, P Scardi and P Maistrelli *J Appl Cryst.* **25** 459 (1992)

[4] L Lutterotti, S K Pradhan, S Gialanella and A R Yavari *Mater. Res. Soc. Symp. Proc* **364** 1077 (1994)

[5] B E Warren *X-ray Diffraction* (Reading, MA · Addision-Wesley) p264 (1969)

[6] C N J Wagner *Local Atomic Arrangements Studied by X-ray Diffraction* (eds) J B Cohen, J E Hilliard (New York Gorden and Breach) p36, ch7 (1966)

[7] H Pal, A Chanda and M De *J Alloys and Compounds* **278** 209 (1998)

[8] S K Pradhan and M De *J Appl Phys.* **64** 2324 (1988)

[9] S K Ghosh and S P Sen Gupta *J. Appl Phys* **56** 1213 (1984)

[10] H Dutta, S K Shee, S K Pradhan and M De *Materials Engg.* **11** 159 (2000)

[11] A Benedetti, G Fagherazzi, S Enzo and M Battagliarin *J Appl Cryst.* **21** 543 (1988)

[12] J G M Van Berkum *Ph D Thesis* (Delft University of Technology, The Netherlands) (1994)

[13] R A Young, D B Wiles *J Appl Cryst* **15** 430 (1982)

[14] R Delhaz, Th H de Keijser, E J Mittemeijer, Z Fresenius *Anal Chem.* **312** 1 (1982)

[15] G K Williamson and R E Smallman *Phil. Mag.* **1** 34 (1956)

[16] L Delehouzee and A Deruyttere *Acta Metall.* **15** 727 (1967)

[17] M Nishida, Y Morizono, T Kai, J Sugimoto, A Chiba and R Kumagae *Materials Transactions JIM* **38** 334 (1997)